JOURNAL OF CHEMICAL INFORMATION AND MODELING

ARTICLE

pubs.acs.org/jcim

Computational Insight into Small Molecule Inhibition of Cyclophilins

Somisetti V. Sambasivarao and Orlando Acevedo*

Department of Chemistry and Biochemistry, Auburn University, Auburn, Alabama 36849, United States

Supporting Information

ABSTRACT: Cyclophilins (Cyp) are a family of cellular enzymes possessing peptidyl-prolyl isomerase activity, which catalyze the *cis*−*trans* interconversion of proline-containing peptide bonds. The two most abundant family members, CypA and CypB, have been identified as valid drug targets for a wide range of diseases, including HCV, HIV, and multiple cancers. However, the development of small molecule inhibitors that possess nM potency and high specificity for a particular Cyp is difficult given the complete conservation of all active site residues between the enzymes. Monte Carlo statistical sampling coupled to free energy perturbation theory (MC/FEP) calculations have been carried out to elucidate the origin of the experimentally observed nM inhibition of CypA by acylurea-based derivatives and the >200-fold in vitro selectivity between CypA and CypB from aryl 1-indanylketone-based μM inhibitors. The computed free-energies of binding were in close accord with those derived from experiments. Binding affinity values for the inhibitors were determined to be dependent upon the stabilization strength of the nonbonded interactions provided toward two catalytic residues: Arg55 and Asn102 in CypA and the analogous Arg63 and Asn110 residues in CypB. Fine-tuning of the hydrophobic interactions allowed for enhanced potency among derivatives. The aryl 1-indanylketones are predicted to differentiate between the cyclophilins by using distinct binding motifs that exploit subtle differences in the active site arrangements. Ideas for the development of new selective compounds with the potential for advancement to low-nanomolar inhibition are presented.

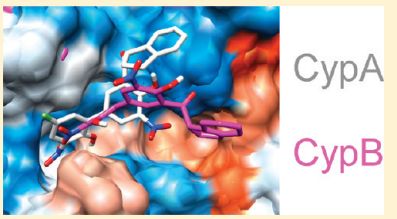

INTRODUCTION

Cyclophilins (Cyp) belong to a class of cellular enzymes possessing peptidyl-prolyl isomerase (PPIase) activity, which catalyze the *cis*−*trans* interconversion of the imide bond in proline residues.[1−5] This isomerization has been identified as the rate-limiting step in protein folding.[6,7] Eight human Cyps with molecular masses ranging from 18 to 150 kDa[7] and an additional 12 multidomain Cyps (masses up to 352 kDa) have been reported to utilize a highly conserved active site making specific inhibition of a particular family member difficult.[8] Of specific interest to this research are human CypA and CypB[9] as both cyclophilins have been identified as valid drug targets for hepatitis C virus (HCV) treatment.[10−17] CypA and CypB are found to interact with the HCV RNA-dependent RNA polymerase NS5B, essential in HCV replication.[18] HCV is a key player in the development of major liver diseases, including liver cirrhosis and hepatocellular carcinoma, and accounts for a significant proportion of hepatitis cases worldwide with most infections becoming chronic, i.e., approximately 60% of patients develop liver disease.[19−21] Unfortunately, the difficulty in treating HCV is attributable to limited therapy options and a substantial risk of premature discontinuation of medication due to side effects.[22]

Cyclosporin A (CsA), a global cyclophilin inhibitor, has been identified to substantially inhibit intracellular HCV replication[1,12,13,23−26], and additional inhibitors derived from natural products and peptide analogs have also been reported, e.g., FK506,[27] rapamycin,[28] sanglifehrin A,[29] and Debio-025.[10] New compounds are urgently needed that selectively bind with cyclophilins in order to reduce side effects; however, controversy surrounds which cyclophilin, CypA or CypB, plays the largest role in HCV replication and hence which one should be targeted for treatment. For example, Watashi et al. recently reported that downregulation of CypB reduced HCV RNA titer, but knockdown of CypA or CypC did not.[11] Conversely, Yang et al. reported that silencing of CypB or CypC expression had no significant effect on replication, but HCV showed a dependency for CypA.[14] Nakagawa et al. determined that knockdown of CypA, CypB, and CypC suppressed HCV replication significantly.[13] It is clear that a detailed atomic-level understanding of the selective inhibition of cyclophilins is needed to treat hepatitis C and to elucidate the role that the enzymes play in HCV replication. In addition, compounds displaying selective inhibition of CypA,[30,31] CypB,[32] CypC,[5,33] or CypD[34] could be extended to treatments of other diseases beyond HCV, including HIV,[35] multiple cancers,[36] e.g., breast,[37,38] pancreatic,[39] and nonsmall cell lung cancers,[40] and inflammatory diseases,[41] such as rheumatoid arthritis.[42]

In the current study, Monte Carlo statistical mechanics simulations utilizing free energy perturbation theory (MC/FEP) have been used to calculate the relative free-energies of binding, $\Delta\Delta G_{bind}$, for multiple potent small molecule inhibitors of CypA and CypB (Figure 1). Atomic-level computer models of the proteins were constructed from high-resolution crystal structures, and the resultant MC/FEP calculations have yielded good agreement with recently reported experimental IC_{50} (in vitro)

Received: October 19, 2010
Published: December 31, 2010

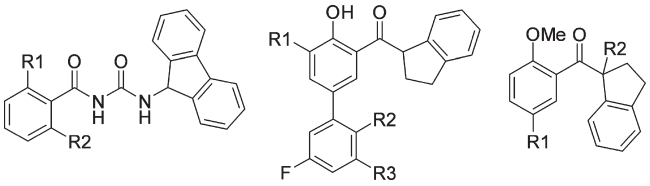

Figure 1. Chemical structures of acylurea-based (**1**) and aryl 1-indanylketone-based (**2** and **3**) cyclophilin inhibitors.

values for substituted acylurea-based compounds (**1**) in CypA[43] and K_i (inhibitory constant) values for multiple variations of aryl 1-indanylketone-based compounds (**2** and **3**) in CypA and CypB.[44] Insight is provided into the origin of the nanomolar inhibitory potency of compound **1** and the observed binding specificity between CypA and CypB by compounds **2** and **3**. The reasons behind the selectivity have been difficult to rationalize from an experimental perspective given the complete conservation of all active site residues between the cyclophilins. An enhanced understanding of the intermolecular interactions occurring in the multiple protein−ligand complexes is given and could aid in the creation of antiviral therapeutics based on small organic inhibitors that display desirable pharmacokinetic and physicochemical characteristics.

COMPUTATIONAL METHODS

The free energy perturbation (FEP) technique serves as the foundation for computing protein−ligand binding affinities in this work. FEP uses the Zwanzig expression (eq 1) to relate the free energy difference between an initial (0) and final (1) state of a system. For relative free energies of binding, single-topology perturbations[45] are made to convert one ligand to another using the thermodynamic cycle shown in Figure 2. The ligand mutations of compounds **1**−**3** used double-wide sampling with 14 FEP windows; a similar methodology was recently reported.[46,47] A window refers to a Monte Carlo (MC) simulation at one point along the mutation coordinate λ, which interconverts two ligands as λ goes from 0 to 1. Double-wide implies that two free energy changes are computed at each window, corresponding to a forward and backward increment. The spacing between the windows, $\Delta\lambda$, is primarily 0.1 with the exception of $\lambda = 0 - 0.2$ and $0.8 - 1$, where the spacing is 0.05, which addresses the fact that the free energy often changes most rapidly in these regions. The difference in free energies of binding for the ligands X and Y then comes from eq 2. Two series of mutations are performed to convert X to Y unbound in water and complexed to the protein which yield ΔG_F and ΔG_C. For recent reviews on the topic and historical perspectives, please see refs 47−49.

$$\Delta G(\mathrm{X} \rightarrow \mathrm{Y}) = -k_B T \ln \langle \exp[-(E_Y - E_X)/k_B T] \rangle_X \quad (1)$$

$$\Delta\Delta G_{bind} = \Delta G_X - \Delta G_Y = \Delta G_F - \Delta G_C \quad (2)$$

Initial Cartesian coordinates for the protein−ligand structures were generated with the molecule-growing program BOMB starting from the PDB files 1awq[50] for CypA and 1cyn[51] for CypB; the existing complexed ligands were removed and replaced by cores such as formaldehyde to grow the desired

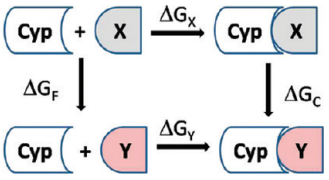

Figure 2. Thermodynamic cycle for relative free energies of binding. Cyp is the cyclophilin receptor, and X and Y are different ligands.

analogues in the binding site. The present models include one active site, the inserted ligand, and all crystal structure residues. Terminal residues were capped with acetyl or N-methylamine groups. The system was then subjected to conjugate-gradient energy minimization in order to relax the contacts between protein residues and the ligand. The total charge of the system was set to zero by adjusting the protonation states of a few residues furthest away from the center of the system. The entire system was solvated with 25-Å caps containing 1250 and 2000 TIP4P water molecules[52] for the protein complexes and unbound ligands, respectively; a half-harmonic potential with a force constant of 1.5 kcal mol^{-1} A^{-2} was applied to water molecules at a distance greater than 25 Å. The MC/FEP calculations were executed with MCPRO.[53] The energetics of the systems were classically described with the OPLS-AA force field for the protein and OPLS/CM1A for the ligands.[54] For the MC simulations, all degrees of freedom were sampled for the ligands, while TIP4P water molecules only translated and rotated; bond angles and dihedral angles for protein side chains were also sampled, while the backbone was kept fixed after the conjugate-gradient relaxation. Each mutation window for the unbound ligands in water consisted minimally of 20 million (M) configurations of MC equilibration followed by 40 M configurations of averaging. For the bound calculations, the equilibration period is minimally 5 M configurations of solvent only moves, followed by 10 M configurations of full equilibration, followed by 20 M configurations of averaging. All MC simulations were carried out at 25 °C. Our recent QM/MM study of catalytic antibody 4B2 used a similar computational setup and produced close agreement with experimental rate data.[55]

In some cases, AUTODOCK 4.2[56] was used to dock the full inhibitors (not cores) into the crystal structures for verification of the binding conformations predicted by BOMB. AutoDockTools (ADT) was used to prepare, run, and analyze the docking simulations. The rigid roots of each ligand were defined automatically, and the amide bonds were made nonrotatable. Polar hydrogens were added, and Gasteiger charges were assigned. Nonpolar hydrogens were subsequently merged. A grid was centered on the catalytic active site region and included all amino acid residues within a box size set at $x = y = z = 40$ Å. AutoGrid 4 was used to produce grid maps with the spacing between the grid points at 0.375 Å. The Lamarckian Genetic Algorithm (LGA) was chosen to search for the best conformers. During the docking process, 50−100 conformers were considered for each compound. The population size was set to 150, and the individuals were initialized randomly. The maximum number of energy evaluation was set to 2500000; default docking parameters were primarily used, for example: maximum number of generations to 27000, maximum number of top individual that automatically survived set to 1, mutation rate of 0.02, crossover rate of 0.8, step sizes were 2 Å for translations, 50° for quaternions, and 50° for torsions, and a cluster tolerance of 2 Å was employed.

Table 1. MC/FEP Results for Mutation of Acylurea-Based Inhibitors (1)[a]

compd	R_1	R_2	$\Delta\Delta G_{bind}$ (calc)	$\Delta\Delta G_{bind}$ (exptl)[b]	IC_{50} (nM)[c]
1a	Cl	F	−1.48 ± 0.07	−3.05	1.52 ± 0.10
1a	F	Cl	8.38 ± 0.26		
1b	Cl	Cl	−1.37 ± 0.10	−2.74	2.59 ± 0.20
1c	CN	H	−0.21 ± 0.16	−0.78	71.2 ± 0.30
1c	H	CN	−1.67 ± 0.19		
1d	Cl	H	−0.68 ± 0.09	−0.56	103 ± 5
1d	H	Cl	1.44 ± 0.10		
1e	F	H	−0.13 ± 0.07	−0.30	159 ± 7
1e	H	F	0.51 ± 0.07		
1f	F	F	0	0	263 ± 24
1g	NO_2	H	0.54 ± 0.30	0.51	620 ± 32
1g	H	NO_2	2.62 ± 0.36		
1h	OH	H	1.67 ± 0.13	>2.15	>10,000
1h	H	OH	1.56 ± 0.14		
1i	NH_2	H	0.05 ± 0.20	>2.15	>10,000
1i	H	NH_2	0.07 ± 0.22		
1j	H	H	0.27 ± 0.09	inactive	inactive

[a] Positive $\Delta\Delta G_{bind}$ value (kcal/mol) means R_1= R_2 = F (1f) was preferred, and negative means new mutation is preferred. [b] Calculated from $\Delta\Delta G_{bind}$ = RT ln [IC_{50}(1x)/IC_{50}(1f)] at 298 K. [c] Experimental IC_{50} values from ref 43

RESULTS AND DISCUSSION

Acylurea-Based Compounds. Configurationally averaged MC/FEP calculations have been carried out by smoothly mutating the acylurea-based scaffold reported by Ni et al.[43] (**1**) to 10 different compounds, **1a**−**1j**, featuring variations of R_1 and R_2 (Figure 1 and Table 1). Table 1 provides the computed $\Delta\Delta G_{bind}$ values with the correct binding affinity trend predicted when compared to the IC_{50} enzyme inhibition assay results. Uncertainties in the $\Delta\Delta G_{bind}$ have been calculated by propagating the standard deviation (σ_i) on the individual ΔG_i values for each $\Delta\lambda$ window. Some deviations from experiments were found, for example, **1j** (R_1 = R_2 = H) was predicted to have a $\Delta\Delta G_{bind}$ value similar to that of **1f** (R_1 = R_2 = F) despite showing no activity in the IC_{50} assay. Ni et al. also predicted **1j** to be active with a computed K_d value of 316 nM using their LigBuilder 2.0 program[43]; the results may suggest a breakdown of the scoring functions or force field. Interestingly, a buried water molecule is located in the hydrophobic subpocket where the phenyl ring of **1j** resides that is not found in **1f** (Figure S1 of the Supporting Information); annihilation of buried waters in enzymes using a double-decoupling method has been shown to improve FEP accuracy in recent work.[57,58] Figure 3 provides images constructed from the last configuration of a MC/FEP calculation for the most potent inhibitor **1a** (R_1 = Cl and R_2 = F) bound to CypA; a hydrophobicity surface is given in Figure 3A ranging from blue for the most polar residues to white to orange-red for the most hydrophobic region (image made using Chimera[59]). The binding mode of compound **1** as predicted by BOMB is consistent with previous motifs generated from AUTODOCK 3 and LigBuilder 2.0, where an rmsd of about 1.5 Å was found between the methods.[43] The tandem amide forms multiple tight hydrogen bond interactions with the Arg55, Gln63, and Asn102 residues located in the "saddle" region of the active site, while the planar fluorene rings and 2,6-disubstituted phenyl moiety of the inhibitors insert favorably into two adjacent hydrophobic sub-binding pockets.

The large differences in the binding affinities of **1** derivatives have been attributed to the groups present on the 2,6-disubstituted phenyl ring, i.e., R_1 or R_2, where the potency is generally improved by the addition of greasy substituents and electron-withdrawing groups.[43] In the present calculations, R_1 and R_2 are not equivalent as they do not interconvert during the MC simulation requiring separate simulations for each "conformer." If only one equivalent position is energetically preferred, then a penalty of RT ln 2 (0.6 kcal/mol) can be expected for loss of one rotameric state upon binding.[46] For example, simulations found that a Cl at the R_1 position of **1a**, which points into a hydrophobic pocket, improved the binding affinity relative to **1f** with a computed $\Delta\Delta G_{bind}$ of −1.48 kcal/mol compared to 8.38 kcal/mol when the Cl points to the bulk phase water, i.e., the R_2 position. While **1a** provided the most extreme preference for the R_1 position, hydrophobic substituents generally improved the binding affinity by pointing into the same sub-binding pocket, whereas hydrophilic groups, like −CN in compound **1c**, preferred to point into the bulk water. Hydrophobic interactions are regarded as one of the key factors leading to improved potency among the **1** derivatives,[43] but the major overall contributor of the measured nanomolar inhibitory values for the scaffold was determined by our calculations to be strong hydrogen bonding interactions between the acylurea portion of the solute and the polar "saddle" residues in the active site.

In a recent study by Hamelberg and McCammon, molecular dynamic simulations were carried out for the *cis*−*trans* isomerization of the −Gly-Pro− ω angle of the Ace-His-Ala-Gly-Pro-Ile-Ala-Nme substrate in CypA.[2] Their simulations concluded that CypA better stabilizes the transition state, ω = 90°, as compared to the *cis* or *trans* isomers by forming long-lasting hydrogen bonds with primarily two residues: Arg55 and Asn102. Gly was determined to form a hydrogen bond with the backbone NH group of Asn102, and Pro formed a hydrogen bond between its carbonyl oxygen and the guanidinium moiety of Arg55. In the current study, the same residues are essential in providing stabilizing interactions with compound **1**, which appears to mimic well the transition state conformation of the −Gly-Pro− substrate. For example, the average distances over the final 20 million MC/FEP configurations between the closest hydrogen on the Arg55 guanidinium moiety and the carbonyl oxygen closest to the 2,6-disubstituted phenyl ring were 2.8, 2.6, and 2.8 Å for the most favorable **1a**, **1f**, and **1h** compounds, respectively (Figure 3B). The hydrogen covalently bonded to nitrogen from Gln63 formed average hydrogen bond distances of 2.8, 3.0, and 3.0 Å with the carbonyl oxygen closest to the phenyl ring for **1a**, **1f**, and **1h**, respectively, and distances of 2.1, 1.9, and 2.0 Å with the carbonyl oxygen nearest the fluorene rings. The average distances between the carbonyl backbone oxygen of Asn102 and the hydrogen covalently bonded to the amide nearest the phenyl ring were 1.9, 2.3, and 1.8 Å for **1a**, **1f**, and **1h**, respectively, and 2.5, 2.1, and 2.3 Å for the amide hydrogen closest to the fluorene rings. A breakdown of the total Coulombic and van der Waals interaction energies between **1a** and the residues finds large values of −11.7 and −10.9 kcal/mol for Arg55 and Asn102, respectively, which is consistent with Hamelberg and McCammon's findings that those two residues are essential in stabilizing the transition state conformation.[2] The next best nonbonded solute−protein interaction energies were for Gln63

dx.doi.org/10.1021/ci1004114 |J. Chem. Inf. Model. 2011, 51, 475–482

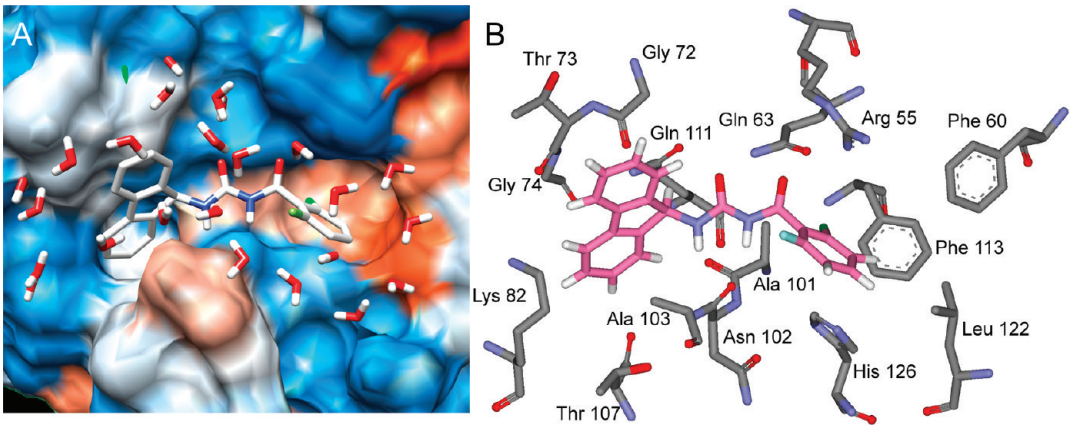

Figure 3. CypA active site and bound acylurea-inhibitor **1a** (R_1 = Cl and R_2 = F) with (A) nearby waters shown and a hydrophobic surface representation where blue is the most polar regions and orange-red is the most hydrophobic, and (B) key residues from the binding site.

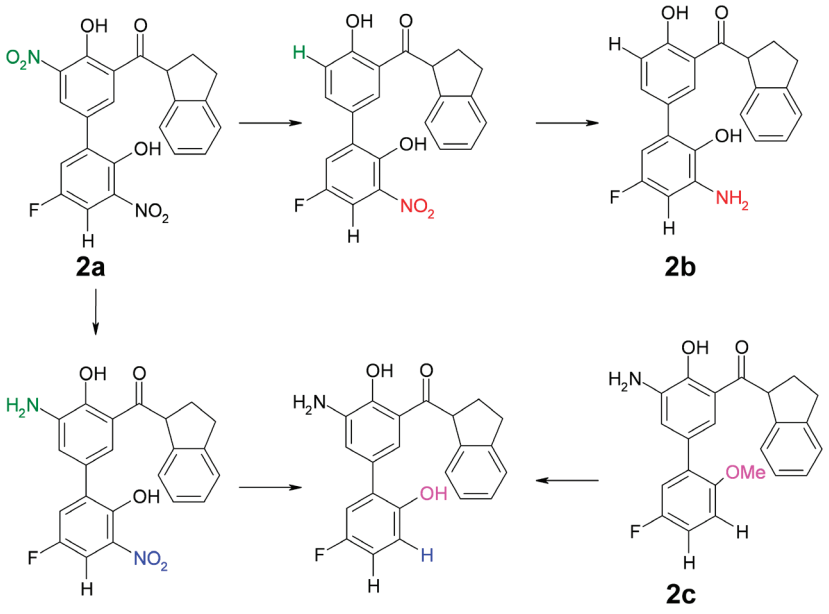

Figure 4. Transformation sequence used in the FEP simulations for the aryl 1-indanylketone-based compounds (**2**).

and Ala103 with values of −5.1 and −5.5 kcal/mol, respectively. However, for compound **1h** (R_1 = OH and R_2 = H) the energetic interactions with Arg55 and Asn102 were reduced to −10.1 and −6.9 kcal/mol, respectively, which is consistent with its reduced binding affinity as compared to the **1a** inhibitor (Table 1). In general, the most favorable acylurea-based derivatives maximize hydrogen bonding with Arg55 and Asn102 and employ favorable hydrophobic interactions within the active site, which may explain the origin of their experimentally observed nanomolar inhibition potency.

Aryl 1-Indanylketone-Based Compounds. A set of compounds based on an aryl 1-indanylketone scaffold (**2**) reported by Daum et al.[44] were also simulated by using the MC/FEP transformation sequence given in Figure 4. The computed $\Delta\Delta G_{bind}$ values in both CypA and CypB (Table 2) were found to yield excellent agreement with the experimental free-energy differences derived from the K_i protease-free PPIase assay at pH 7.8 and 283 K.[44] The indanylketone-based compounds, **2a**−**2c**, have reduced μM inhibition K_i values for the cyclophilins when compared to the nM potency of the acylurea-based **1** compounds (Tables 1 and 2). The present calculations on **2a**−**2c** continue to lend support to the idea that the binding affinity is tied to the ability of the inhibitor to stabilize Arg55 and Asn102 in CypA and

Table 2. MC/FEP Results for Mutation of Aryl 1-Indanylketone Inhibitors (2)

compd	$\Delta\Delta G_{bind}$ (calc)	$\Delta\Delta G_{bind}$ (exptl) [a]	K_i (μM)[b]
	CypA		
2a	−0.61 ± 0.55	−0.67	0.52 ± 0.15
2b	−1.44 ± 0.69	−0.98	0.3 ± 0.1
2c	0.0	0.0	1.7 ± 0.5
	CypB		
2a	1.51 ± 0.64	>1.38	>100
2b	0.19 ± 0.58	0.19	12 ± 5
2c	0.0	0.0	8.6 ± 0.9

[a] Calculated from $\Delta\Delta G_{bind}$ = RT ln [K_i(2x)/K_i(2c)] at 283 K. [b] Experimental K_i values from ref 44.

dx.doi.org/10.1021/ci1004114 |J. Chem. Inf. Model. 2011, 51, 475–482

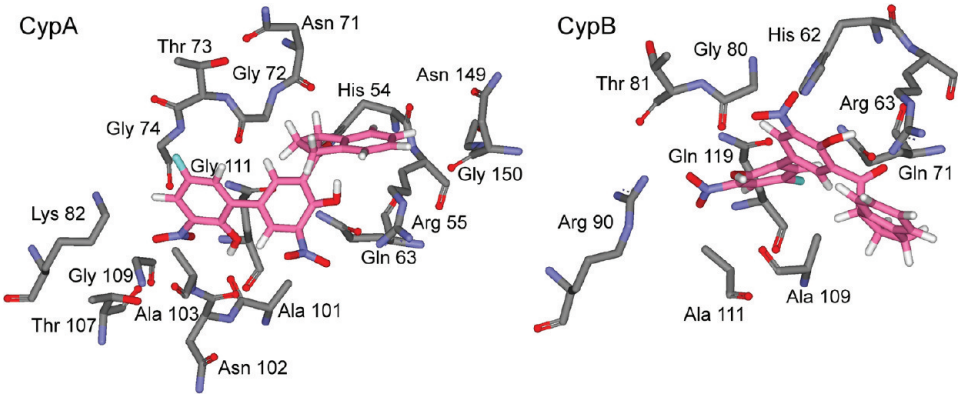

Figure 5. Aryl 1-indanylketone inhibitor **2a** bound to the active site of CypA (left) and CypB (right) with key residues is shown. Nearby waters are removed for clarity.

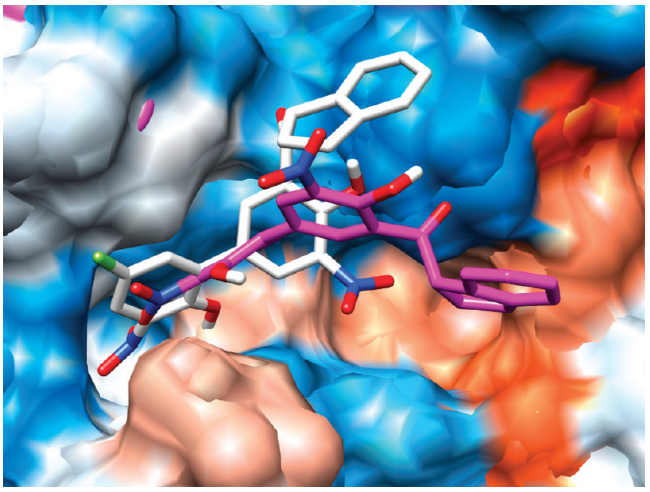

Figure 6. Overlaid CypA (gray) and CypB (pink) active sites with inhibitor **2a** bound at the active sites. Nearby waters are removed for clarity.

the analogous Arg63 and Asn110 residues in CypB. For example, the final 40 million MC/FEP configurations between the closest hydrogen on the Arg55 guanidinium moiety in CypA and oxygen of the nitro group nearest the **2a** indanyl ring found an average distance of 2.6 Å and a Coulombic and van der Waals interaction total energy of −16.3 kcal/mol between the ligand and the residue (Figure 5). However, a significantly weakened nonbonded interaction energy of −4.6 kcal/mol between **2a** and Asn102 is consistent with the reduced μM potency observed when compared to the stronger interaction energies found for the **1a** nM inhibitor. Ala101, Gly72, and Lys82 in CypA also provided additional stabilizing nonbonded interactions with protein−solute energies of about −5.1 to −5.4 kcal/mol via hydrogen bonds; for example, an average distance of 1.9 Å was found between the backbone carbonyl oxygen of Ala101 and the **2a** hydroxyl group on the ring furthest from the indanyl ring.

Compound **2a** is particularly interesting because its K_i value is reported to be 0.52 ± 0.15 μM in CypA and >100 μM in CypB, implying a >200-fold selectivity between the cyclophilins from in vitro and in vivo experiments despite a completely conversed active site.[44] The reasons behind the selectivity have been difficult to rationalize from an experimental perspective. Our calculations suggest that differences in the most favorable binding motifs for **2a** in CypA and CypB may be responsible for the observed selectivity. Figure 6 shows two binding modes for **2a** in the overlaid CypA and CypB active sites, where the structure colored in gray is the preferred binding conformation in CypA and the structure in pink is favored in CypB (**2b** and **2c** are given in Figure S2 of the Supporting Information). It is clear from the figures that the major difference is the orientation of the indanyl ring: CypB prefers a binding motif where the indanyl ring is located in a hydrophobic sub-binding pocket, while CypA has the indanyl ring pointing into a polar region with the adjacent carbonyl oxygen oriented toward His54 (although the nonbonded interactions between **2a** and His54 are weak, as the total energy is −1.7 kcal/mol). Multiple FEP simulations were attempted from different starting geometries, but the reported structures were determined to be the most favorable as other configurations would exit the active site during the MC/FEP simulations or produce very poor energy evaluations. Autodock 4.2 calculations have been carried out to validate the poses predicted by BOMB, and good agreement was found. For example, **2a** was predicted to bind to CypA in conformations similar to that of Figures 5and 6 and Figure S2 of the Supporting Information, and the free-energies of binding were predicted to be more negative than in CypB. Examples of the most relevant poses in CypA and CypB from the docking calculations are provided for comparison in Figures S3 and S4 of the Supporting Information.

The weak binding of **2a** in CypB as compared to that of CypA is tied to poorer interactions between the ligand and the Arg63 and Asn110 residues. The final 40 million MC/FEP configurations between the closest hydrogen on the Arg63 guanidinium moiety in CypB to the oxygen of the carbonyl group nearest the **2a** indanyl ring found an average distance of 3.2 Å and a Coulombic and van der Waals interaction total energy of 0.0 kcal/mol between the ligand and the residue (Figure 5). The total nonbonded interaction energy between **2a** and Asn110 from CypB was −1.9 kcal/mol. The most favorable **2a**−CypB residue interaction was between Arg90 and the nitro group on the ring furthest away from the indanyl ring with a nonbonded interaction energy value of −10.7 kcal/mol. In addition, two waters formed average hydrogen bond distances of about 2.0 Å with the two hydroxyl groups present in **2a**, whereas waters were not required for ligand stabilization in CypA.

The aryl 1-indanylketones have been shown to behave as transition state inhibitors of Pin1, a PPIase of a different family,

dx.doi.org/10.1021/ci1004114 |J. Chem. Inf. Model. 2011, 51, 475–482

Table 3. MC/FEP Results for Mutation of Aryl 1-Indanylketone Inhibitors (3)

compd	$\Delta\Delta G_{bind}$ (calc)	$\Delta\Delta G_{bind}$ (exptl)[a]	K_i (μM)[b]
	CypA		
3a	0.0	0.0	10 ± 2
(S)-**3b**	4.64 ± 0.24	>1.29	>100
(R)-**3b**	−0.88 ± 0.21	−0.16	7.5 ± 1.5
	CypB		
3a	0.0	0.0	>100
(S)-**3b**	0.09 ± 0.21	−	>100
(R)-**3b**	−0.34 ± 0.25	<−0.52	40 ± 10

[a] Calculated from $\Delta\Delta G_{bind}$ = RT ln [K_i(3x)/K_i(3a)] at 283 K. [b] Experimental K_i values from ref 44.

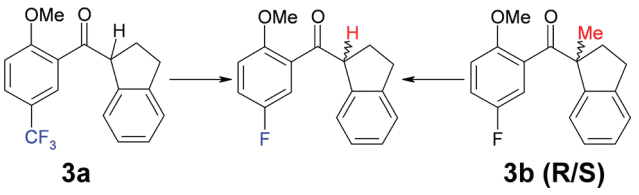

Figure 7. Transformation sequence used in FEP simulations for the aryl 1-indanylketone-based compounds (3).

by mimicking the "twisted-amide" transition state of peptidyl-prolyl structures.[60] The current simulations suggest that **2a** also mimics the transition state in the active site of the cyclophilins and fine-tune their selectivity for CypA by weakening their nonbonded interactions with the catalytic Arg and Asn residues in CypB while simultaneously strengthening them in CypA. The computed functional differences in the residue distances when bound to **2a** are consistent with NMR studies, suggesting that the active site of CypB may exhibit structural differences as compared to CypA during transition state catalysis.[61]

Further variations in the aryl 1-indanylketone scaffold included the substitution of the biphenyl ring with a single phenyl moiety (**3** from Figure 1) that also yielded selectivity between CypA and CypB. For example, compound **3a** is about 10-fold more selective for CypA with a K_i value of 10 ± 2 μM compared to >100 μM in CypB (Table 3).[44] While not as impressive as the 200-fold selectivity of **2a**, a more detailed understanding could aid in the development of new inhibitors. MC/FEP mutations, as shown in Figure 7, were carried out for **3a** and the enantiomeric **3b** compounds, and good agreement with the experimental $\Delta\Delta G_{bind}$ values was found (Table 3). Figure 8 shows comparable binding modes for **3a** in the overlaid CypA and CypB active sites, with the indanyl ring pointing into the polar active site saddle region in an orientation similar to that of **2a** in CypA. Autodock calculations predicted binding poses for **3a** in CypA and CypB similar to that of BOMB and the most favorable binding modes of **2a** (Figures S6 and S7 of the Supporting Information).

The average distance of the final 40 million MC/FEP configurations between the closest hydrogen on the Arg55 guanidinium moiety in CypA and oxygen of the **3a** carbonyl group was 4.2 Å, and a combined Coulombic and van der Waals nonbonded interaction energy of −4.6 kcal/mol was found. The Asn102 residue−**3a** ligand total nonbonded interaction energy was −0.1 kcal/mol. The reduced interactions of **3a** with the catalytic Arg55 and Asn102 residues compared to those of **2a** appear

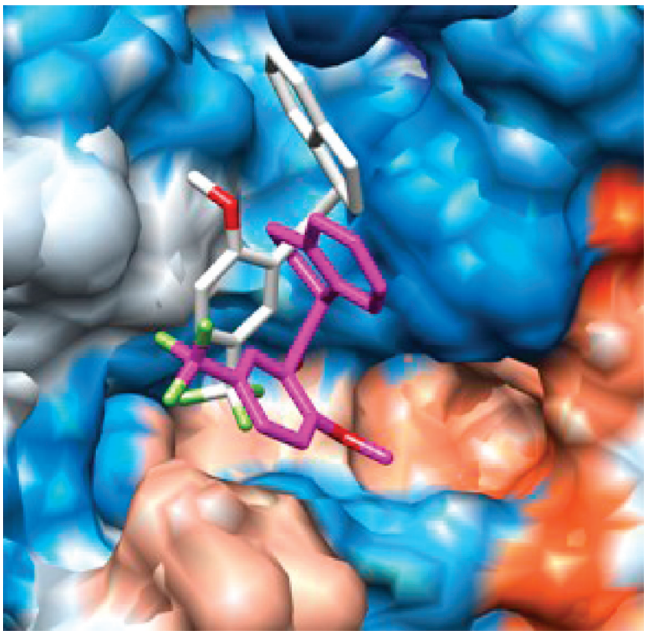

Figure 8. Overlaid CypA (gray) and CypB (pink) active sites with inhibitor **3a** bound at the active sites. Nearby waters are removed for clarity.

consistent with the reduction in K_i from 0.52 to 10 μM from **2a** and **3a** in CypA, respectively. Differences in the orientation of **3a** in the active site of CypB (Figure 8) resulted in a total nonbonded interaction energy of −2.1 kcal/mol with Arg63 and −0.2 kcal/mol with Asn110, which agrees with the observed >100 μM inhibition. The considerable variation in the inhibition of CypA and CypB by the enantiomeric **3b** compounds was also well reproduced (Table 3). The discrepancy in binding affinity can be attributed to space requirements for the methyl group within the active site that resulted in an unfavorable docking motif change for (S)-**3b** as compared to (R)-**3b**. Overlays of (S)-**3b** and (R)-**3b** in CypA and CypB are given in Figure S5 of the Supporting Information .

CONCLUSIONS

MC/FEP calculations have been carried out on a varied set of nM to μM inhibitors of cyclophilins A and B based on acylurea and aryl 1-indanylketone small molecule scaffolds reported by Li[43] and Schiene-Fischer,[44] respectively, in order to elucidate the origin of their potency and specificity. The computed $\Delta\Delta G_{bind}$ values were in close agreement with experimental values derived from IC_{50} and K_i enzyme inhibition assay results. The present simulations find the nM inhibition of CypA from the acylurea-based derivatives, **1**, is primarily the result of favorable stabilization of residues Arg55 and Asn102 via nonbonded interactions. In addition, the planar fluorene rings and 2,6-disubstituted phenyl moiety of the **1** inhibitors inserted favorably into two adjacent hydrophobic sub-binding pockets; the inclusion of hydrophobic groups, e.g., Cl, on the phenyl ring was beneficial as it imparted positive hydrophobic interactions and displaced buried water molecules from the active site. However, any substitutions to the phenyl ring that resulted in the destabilization of the Coulombic or van der Waals interactions between the inhibitor and catalytic Arg and Asn residues resulted in a loss of binding affinity. In addition, the excellent agreement between the

dx.doi.org/10.1021/ci1004114 |J. Chem. Inf. Model. 2011, 51, 475–482

computed and experimentally derived $\Delta\Delta G_{bind}$ for the μM aryl 1-indanylketones, **2** and **3**, inhibitors also supported the theory of the inhibitor binding affinity being tied to the stabilization of the conserved active site Arg and Asn residues in CypA and CypB.

The **2a** aryl 1-indanylketone inhibitor is able to deliver a >200-fold selectivity between CypA and CypB and was predicted from our calculations to differentiate between the cyclophilins by using distinct binding motifs that exploit subtle differences in the active site arrangements. Previous NMR studies have also suggested that the active site of CypB may exhibit structural differences as compared to CypA during transition state catalysis[61], and the current simulations indicate that **2a** and **3a** take advantage of these subtle differences via different binding motifs that fine-tune their selectivity for CypA by exclusively weakening their non-bonded interactions with the catalytic Arg63 and Asn110 residues in CypB. A joint computational and experimental study is currently underway that explores small molecule hybrid structures of **1**, **2**, and **3**, and novel scaffolds that mimic the "twisted-amide" transition state of peptidyl-prolyl structures in the active site with the goal of obtaining selectivity between CypA and CypB with low-nanomolar inhibition potency.

■ ASSOCIATED CONTENT

Supporting Information. Additional hydrophobic surface representations of CypA and CypB with **2** and **3** derivatives bound at the active site from MC/FEP simulations and Autodock calculations of **2** and **3** derivatives in CypA and CypB. This material is available free of charge via the Internet at http://pubs.acs.org.

■ AUTHOR INFORMATION

Corresponding Author

*E-mail: orlando.acevedo@auburn.edu.

■ ACKNOWLEDGMENT

Gratitude is expressed to Auburn University for support of this research. This research was stimulated by discussions with Prof. Patrick Flaherty.

■ REFERENCES

(1) Handschumacher, R. E.; Harding, M. W.; Rice, J.; Drugge, R. J.; Speicher, D. W. Cyclophilin: A specific cytosolic binding protein for cyclosporin A. *Science* **1984**, *226*, 544–547.

(2) Hamelberg, D.; McCammon, J. A. Mechanistic insight into the role of transition-state stabilization in cyclophilin A. *J. Am. Chem. Soc.* **2009**, *131*, 147–152.

(3) Fraser, J. S.; Clarkson, M. W.; Degnan, S. C.; Erion, R.; Kern, D.; Alber, T. Hidden alternative structures of proline isomerase essential for catalysis. *Nature* **2009**, *462*, 669–674.

(4) Ke, H.; Zhao, Y.; Luo, F.; Weissman, I.; Friedman, J. Crystal structure of murine cyclophilin C complexed with immunosuppressive drug cyclosporin A. *Proc. Natl. Acad. Sci. U.S.A.* **1993**, *90*, 11850–11854.

(5) Schneider, H.; Charara, N.; Schmitz, R.; Wehrli, S.; Mikol, V.; Zurini, M. G. M.; Quesniaux, V. F. J.; Movva, N. R. Human cyclophilin C: Primary structure, tissue distribution, and determination of binding specificity for cyclosporins. *Biochemistry* **1994**, *33*, 8218–8224.

(6) Schreiber, S. L. Chemistry and biology of the immunophilins and their immunosuppressive ligands. *Science* **1991**, *251*, 283–287.

(7) Göthel, S. F.; Marahiel, M. A. Peptidyl-prolyl cis−trans isomerases: A superfamily of ubiquitous folding catalysts. *Cell. Mol. Life Sci.* **1999**, *55*, 423–436.

(8) Fischer, G.; Aumüller, T. Regulation of peptide bond cis/trans isomerization by enzyme catalysis and its implication in physiological processes. *Rev. Physiol. Biochem. Pharmacol.* **2003**, *148*, 105–150.

(9) Dornan, J.; Taylor, P.; Walkinshaw, M. D. Structures of immunophilins and their ligand complexes. *Curr. Top. Med. Chem.* **2003**, *3*, 1392–1409.

(10) Flisiak, R.; Horban, A.; Gallay, P.; Bobardt, M.; Selvarajah, S.; Wiercinska-Drapalo, A.; Siwak, E.; Cielniak, I.; Higersberger, J.; Kierkus, J.; Aeschlimann, C.; Grosgurin, P.; Nicolas-Métral, V.; Dumont, J.-M.; Porchet, H.; Crabbé, R.; Scalfaro, P. The cyclophilin inhibitor Debio-025 shows potent anti-hepatitis C effect in patients coinfected with hepatitis C and human immunodeficiency virus. *Hepatology* **2008**, *47*, 817–826.

(11) Watashi, K.; Ishii, N.; Hijikata, M.; Inoue, D.; Murata, T.; Miyanari, Y.; Shimotohno, K. Cyclophilin B is a functional regulator of hepatitis C virus RNApolymerase. *Mol. Cell* **2005**, *19*, 111–122.

(12) Watashi, K.; Hijikata, M.; Hosaka, M.; Yamaji, M.; Shimotohno, K. Cyclosporin A suppresses replication of hepatitis C virus genome in cultured hepatocytes. *Hepatology* **2003**, *38*, 1282–1288.

(13) Nakagawa, M.; Sakamoto, N.; Tanabe, Y.; Koyama, T.; Itsui, Y.; Takeda, Y.; Chen, C. H.; Kakinuma, S.; Ooka, S.; Maekawa, S.; Enomoto, N.; Watanabe, M. Suppression of hepatitis C virus replication by cyclosporin A is mediated by blockade of cyclophilins. *Gastroenterology* **2005**, *129*, 1031–1041.

(14) Yang, F.; Robotham, J. M.; Nelson, H. B.; Irsigler, A.; Kenworthy, R.; Tang, H. Cyclophilin A is an essential cofactor for hepatitis C virus infection and the principal mediator of cyclosporine resistance in vitro. *J. Virol.* **2008**, *82*, 5269–5278.

(15) Watashi, K.; Ishii, N.; Hijikata, M.; Inoue, D.; Murata, T.; Miyanari, Y.; Shimotohno, K. Treating hepatitis C: Can you teach old dogs new tricks? *Hepatology* **2005**, *42*, 1455–1458.

(16) Jarvis, L. M. The waiting game. *C&EN* **2010**, *88*, 12–17.

(17) Tang, H. Cyclophilin inhibitors as a novel HCV therapy. *Viruses* **2010**, *2*, 1621–1634.

(18) Lohmann, V.; Korner, F.; Herian, U.; Bartenschlager, R. Biochemical properties of hepatitis C virus NS5B RNA-dependent RNA polymerase and identification of amino acid sequence motifs essential for enzymatic activity. *J. Virol.* **1997**, *71*, 8416–8428.

(19) Tang, H.; Grise, H. Cellular and molecular biology of HCV infection and hepatitis. *Clin. Science* **2009**, *117*, 49–65.

(20) Cuthbert, J. A. Hepatitis C: Progress and problems. *Clin. Microbiol. Rev.* **1994**, *7*, 505–532.

(21) Liang, T. J.; Jeffers, L. J.; Reddy, K. R.; Medina, M. D.; Parker, I. T.; Cheinquer, H.; Idrovo, V.; Rabassa, A.; Schiff, E. R. Viral pathogenesis of hepatocellular carcinoma in the United States. *Hepatology* **1993**, *18*, 1326–1333.

(22) Martinot-Peignoux, M.; Boyer, N.; Pouteau, M.; Castelnau, C.; Giuily, N.; Duchatelle, V.; Aupérin, A.; Degott, C.; Benhamou, J.-P.; Erlinger, S.; Marcellin, P. Predictors of sustained response to alpha interferon therapy in chronic hepatitis C. *J. Hepatol.* **1998**, *29*, 214–223.

(23) Nakagawa, M.; Sakamoto, N.; Enomoto, N.; Tanabe, Y.; Kanazawa, N.; Koyama, T.; Kurosaki, M.; Maekawa, S.; Yamashiro, T.; Chen, C.-H.; Itsui, Y.; Kakinuma, S.; Watanabe, M. Specific inhibition of hepatitis C virus replication by cyclosporin A. *Biochem. Biophys. Res. Commun.* **2004**, *313*, 42–47.

(24) Kofron, J. L.; Kuzmic, P.; Kishore, V.; Colon-Bonilla, E.; Rich, D. H. Determination of kinetic constants for peptidyl prolyl cis-trans isomerases by an improved spectrophotometric assay. *Biochemistry* **1991**, *30*, 6127–6134.

(25) Inoue, K.; Sekiyama, K.; Yamada, M.; Watanabe, T.; Yasuda, H.; Yoshiba, M. Combined interferon α2b and cyclosporin A in the treatment of chronic hepatitis C: Controlled trial. *J. Gastroenterol.* **2003**, *38*, 567–572.

(26) Inoue, K.; Yoshiba, M. Interferon combined with cyclosporine treatment as an effective countermeasure against hepatitis C virus recurrence in liver transplant patients with end-stage hepatitis C virus related disease. *Transplant. Proc.* **2003**, *37*, 1233–1234.

(27) Siekierka, J. J.; Hung, S. H. Y.; Poe, M.; Lin, C. S.; Sigal, N. H. A cytosolic binding protein for the immunosuppressant FK506 has

peptidyl-prolyl isomerase activity but is distinct from cyclophilin. *Nature* **1989**, *341*, 755–757.

(28) Calne, R. Y.; Lim, S.; Samaan, A.; Collier, D. S. J.; Pollard, S. G.; White, D. J. G.; Thiru, S. Rapamycin for immunosuppression in organ allografting. *Lancet* **1989**, *334*, 227.

(29) Sedrani, R.; Kallen, J.; Cabrejas, L. M. M.; Papageorgiou, C. D.; Senia, F.; Rohrbach, S.; Wagner, D.; Thai, B.; Eme, A.-M. J.; France, J.; Oberer, L.; Rihs, G.; Zenke, G.; Wagner, J. Sanglifehrin−cyclophilin interaction: Degradation work, synthetic macrocyclic analogues, X-ray crystal structure, and binding data. *J. Am. Chem. Soc.* **2003**, *125*, 3849–3859.

(30) Kallen, J.; Spitzfaden, C.; Zurini, M. G. M.; Wider, G.; Widmer, H.; Wuthrich, K.; Walkinshaw, M. D. Structure of human cyclophilin and its binding site for cyclosporin A determined by X-ray crystallography and NMR spectroscopy. *Nature* **1991**, *353*, 276–279.

(31) Ke, H. M.; Zydowsky, L. D.; Liu, J.; Walsh, C. T. Crystal structure of recombinant human T-cell cyclophilin A at 2.5 A resolution. *Proc. Natl. Acad. Sci. U.S.A.* **1991**, *88*, 9483–9487.

(32) Price, E. R.; Zydowsky, L. D.; Jin, M. J.; Baker, C. H.; McKeon, F. D.; Walsh, C. T. Human cyclophilin B: A second cyclophilin gene encodes a peptidyl-prolyl isomerase with a signal sequence. *Proc. Natl. Acad. Sci. U.S.A.* **1991**, *88*, 1903–1907.

(33) Friedman, J.; Weissman, I. Two cytoplasmic candidates for immunophilin action are revealed by affinity for a new cyclophilin: One in the presence and one in the absence of CsA. *Cell* **1991**, *66*, 799–806.

(34) Kajitani, K.; Fujihashi, M.; Kobayashi, Y.; Shimizu, S.; Tsujimoto, Y.; Miki, K. Crystal structure of human cyclophilin D in complex with its inhibitor, cyclosporin A at 0.96-Å resolution. *Proteins* **2008**, *70*, 1635–1639.

(35) Luban, J.; Bossolt, K. L.; Franke, E. K.; Kalpana, G. V.; Goff, S. P. Human immunodeficiency virus type 1 Gag protein binds to cyclophilins A and B. *Cell* **1993**, *73*, 1067–1078.

(36) Yao, Q.; Li, M.; Yang, H.; Chai, H.; Fisher, W.; Chen, C. Roles of cyclophilins in cancers and other organ systems. *World J. Surg.* **2005**, *29*, 276–280.

(37) Zheng, J.; Koblinski, J. E.; Dutson, L. V.; Feeney, Y. B.; Clevenger, C. V. Prolyl isomerase cyclophilin A regulation of Janus-activated kinase 2 and the progression of human breast cancer. *Cancer Res.* **2008**, *68*, 7769–7778.

(38) Fang, F.; Flegler, A. J.; Du, P.; Lin, S.; Clevenger, C. V. Expression of cyclophilin B is associated with malignant progression and regulation of genes implicated in the pathogenesis of breast cancer. *Am. J. Pathol.* **2009**, *174*, 297–308.

(39) Shen, J.; Person, M. D.; Zhu, J.; Abbruzzese, J. L.; Li, D. Protein expression profiles in pancreatic adenocarcinoma compared with normal pancreatic tissue and tissue affected by pancreatitis as detected by two-dimensional gel electrophoresis and mass spectrometry. *Cancer Res.* **2004**, *64*, 9018–9026.

(40) Howard, B. A.; Zheng, Z.; Campa, M. J.; Wang, M. Z.; Sharma, A.; Haura, E.; Herndon, J. E., II; Fitzgerald, M. C.; Bepler, G.; Patz, E. F., Jr Translating biomarkers into clinical practice: Prognostic implications of cyclophilin A and macrophage migratory inhibitory factor identified from protein expression profiles in nonsmall cell lung cancer. *Lung Cancer* **2004**, *46*, 313–323.

(41) Arora, K.; Gwinn, W. M.; Bower, M. A.; Watson, A.; Okwumabua, I.; MacDonald, H. R.; Bukrinsky, M. I.; Constant, S. L. Extracellular cyclophilins contribute to the regulation of inflammatory responses. *J. Immunol.* **2005**, *175*, 517–522.

(42) Billich, A.; Winkler, G.; Aschauer, H.; Rot, A.; Peichl, P. Presence of cyclophilin A in synovial fluids of patients with rheumatoid arthritis. *J. Exp. Med.* **1997**, *185*, 975–980.

(43) Ni, S.; Yuan, Y.; Huang, J.; Mao, X.; Lv, M.; Zhu, J.; Shen, X.; Pei, J.; Lai, L.; Jiang, H.; Li, J. Discovering potent small molecule inhibitors of cyclophilin A using de novo drug design approach. *J. Med. Chem.* **2009**, *52*, 5295–5298.

(44) Daum, S.; Schumann, M.; Mathea, S.; Aumller, T.; Balsley, M. A.; Constant, S. L.; Lacroix, B. F. d.; Kruska, F.; Braun, M.; Schiene-Fischer, C. Isoform-specific inhibition of cyclophilins. *Biochemistry* **2009**, *48*, 6268–6277.

(45) Jorgensen, W. L.; Ravimohan, C. Monte Carlo simulation of differences in free energies of hydration. *J. Chem. Phys.* **1985**, *83*, 3050–3054.

(46) Zeevaart, J. G.; Wang, L.; Thakur, V. V.; Leung, C. S.; Tirado-Rives, J.; Bailey, C. M.; Domaoal, R. A.; Anderson, K. S.; Jorgensen, W. L. Optimization of azoles as anti-human immunodeficiency virus agents guided by free-energy calculations. *J. Am. Chem. Soc.* **2008**, *130*, 9492–9499.

(47) Jorgensen, W. L. Efficient drug lead discovery and optimization. *Acc. Chem. Res.* **2009**, *42*, 724–733.

(48) Straatsma, T. P.; McCammon, J. A. Computational alchemy. *Annu. Rev. Phys. Chem.* **1992**, *43*, 407–435.

(49) Jorgensen, W. L.; Thomas, L. L. Perspective on free-energy perturbation calculations for chemical equilibria. *J. Chem. Theory Comput.* **2008**, *4*, 869–876.

(50) Vajdos, F. F.; Yoo, S.; Houseweart, M.; Sundquist, W. I.; Hill, C. P. Crystal structure of cyclophilin A complexed with a binding site peptide from the HIV-1 capsid protein. *Protein Sci.* **1997**, *6*, 2297–2307.

(51) Mikol, V.; Kallen, J.; Walkinshaw, M. D. X-ray structure of a cyclophilin B/cyclosporin complex: comparison with cyclophilin A and delineation of its calcineurin-binding domain. *Proc. Natl. Acad. Sci. U.S.A.* **1994**, *91*, 5183–5186.

(52) Jorgensen, W. L.; Chandrasekhar, J.; Madura, J. D.; Impey, W.; Klein, M. L. Comparison of simple potential functions for simulating liquid water. *J. Chem. Phys.* **1983**, *79*, 926–935.

(53) Jorgensen, W. L.; Tirado-Rives, J. Molecular modeling of organic and biomolecular systems using BOSS and MCPRO. *J. Comput. Chem.* **2005**, *26*, 1689–1700.

(54) Jorgensen, W. L.; Tirado-Rives, J. Potential energy functions for atomic-level simulations of water and organic and biomolecular systems. *Proc. Natl. Acad. Sci. U.S.A.* **2005**, *102*, 6665–6670.

(55) Acevedo, O. Role of water in the multifaceted catalytic antibody 4B2 for allylic isomerization and Kemp elimination reactions. *J. Phys. Chem. B* **2009**, *113*, 15372–15381.

(56) Morris, G. M.; Huey, R.; Lindstrom, W.; Sanner, M. F.; Belew, R. K.; Goodsell, D. S.; Olson, A. J. AutoDock4 and AutoDockTools4: Automated docking with selective receptor flexibility. *J. Comput. Chem.* **2009**, *30*, 2785–2791.

(57) Michel, J.; Tirado-Rives, J.; Jorgensen, W. L. Energetics of displacing water molecules from protein binding sites: Consequences for ligand optimization. *J. Am. Chem. Soc.* **2009**, *131*, 15403–15411.

(58) Gilson, M. K.; Given, J. A.; Bush, B. L.; McCammon, J. A. The statistical-thermodynamic basis for computation of binding affinities: A critical review. *Biophys. J.* **1997**, *72*, 1047–1069.

(59) Pettersen, E. F.; Goddard, T. D.; Huang, C. C.; Couch, G. S.; Greenblatt, D. M.; Meng, E. C.; Ferrin, T. E. UCSF Chimera: A visualization system for exploratory research and analysis. *J. Comput. Chem.* **2004**, *13*, 1605–1612.

(60) Daum, S.; Erdmann, F.; Fischer, G.; Féaux de Lacroix, B.; Hessamian-Alinejad, A.; Houben, S.; Frank, W.; Braun, M. Aryl indanyl ketones: Efficient inhibitors of the human peptidyl prolyl cis/trans isomerase Pin1. *Angew. Chem., Int. Ed.* **2006**, *45*, 7454–7458.

(61) Neri, P.; Gemmecker, G.; Zydowsky, L. D.; Walsh, C. T.; Fesik, S. W. NMR studies of [U-13C]cyclosporin A bound to human cyclophilin B. *FEBS Lett.* **1991**, *290*, 195–199.